16 Disordered and Biological Soft Matter

M. Ackermann, C. M. Aegerter, F. Atzeni, P. Dagenais (since September 2015), D. Dreher, D. Eder, A. Keller, F. Lanfranconi, A. Mallavalli, A. Pataki (Master student), S. Puri, R. Rüttimann (Master student), L. Schertel (since April 2015), J. Schneider, L. Selvaggi and S. Urdy

in collaboration with: Institute of Molecular Life Sciences (K. Basler, T. Aegerter-Wilmsen, L. Pelkmans, D. Brunner), ETH Zürich (P. Koumoutsakos), MPI für Planzenforschung Köln (R.S. Smith), University of Fribourg (A. Jazwinska), University of Bern (C. Kulemeier, S. Robinson), Biozentrum Basel (M. Affolter), University of Konstanz (G. Aubry, G. Maret), MPI für Selbstorganisation Göttingen (C.C. Maass), Deutsches Luft- und Raumfahrtzentrum (M. Sperl), University of Twente (A. Mosk), Université Joseph Fourier Grenoble (S. Skipetrov), Université Paris Denis Diderot (F. Graner), Technion Haifa (E. Akkermans).

The group of disordered and biological soft-matter investigates the behaviour of disordered materials outside of thermal equilibrium, where instabilities arise that lead to emergent structures. Specifically, three overarching themes are currently studied: The first is focussing on light transport in disordered, multiple-scattering media. This is carried out in connection to Anderson localization, which appears in the case of extreme disorder and which we have studied in detail. In addition, other fundamental properties of multiple-scattering transport are studied, such as the influence of the breaking of path-reciprocity in Faraday-active materials. On the more applied side, the understanding of multiple scattering processes is used to create novel microscopy techniques that are capable of compensating the turbidity using wave-front shaping. Such novel imaging techniques are also developed for use in the second class of problems where the regulation of biological development via mechanical forces is investigated. This is studied in the growth of the Drosophila wing and its folds as well as in the regeneration of fins of the zebrafish. Besides studying the direct growth regulation, the control of developmental processes by mechanical forces is also investigated in the context of shaping three dimensional structures as a driver of morphogenesis. The process of dorsal closure in Drosophila embryos is used for this study. As a complement to these biological systems physical model systems far outside of equilibrium, such as granular gases and foams are investigated. These are studied in diamagnetic levitation in order to obtain information on long time dynamics, which is otherwise masked by the effects of gravity. This allows to understand overall properties of instabilities in disordered non-equilibrium systems.

In the last year, we have made progress in several of these areas, which are discussed in detail below. These subjects concern multiple-scatting Faraday-active materials, imaging in turbid media, as well as the development of molecular force sensors to study the force distributions in tissues, such as the Drosophila wing imaginal disc.

16.1 Multiple Scattering in Faraday-active Materials

Wave propagation in multiple scattering media shows various coherent phenomena connected to the localization of the wave transport, first described by Anderson almost 60 years ago [1]. One aspect, known as weak localization is manifest in the enhancement of multiple scattered light in the direct back direction, known as coherent backscattering [2–4]. These coherent effects are closely connected to the concept of reciprocity on multiply scattering paths, leading to constructive interference. Manipulating the path-reciprocity in such media is a powerful tool to study these phenomena in experiments [5]. In optical experiments, this can be achieved by using Faraday active materials as scattering media and carrying out the experiments in high magnetic fields. It is then possible to destroy the coherence even in strongly scattering samples with a mean free path ℓ^* in the μm range, see Fig. 16.1, provided the Faraday rotation of the sample is strong enough. For this purpose, high magnetic fields of 18 T and low temperatures (T < 10 K) are necessary. These experiments were carried out in TiO_2 samples containing Faraday active CeF_3. In addition to the coherent backscattering cone (CBC) shown in Fig. 16.1, these effects can also be studied in a transmission geometry by investigating the speckle correlation functions [6], where a combination of these two different experiments allows for a quantitative determination of the Verdet constant in the multiple scattering regime. In the extreme case of high magnetic fields and low temperaturess, shown in Fig. 16.2, we have been able to observe the onset of saturation of Faraday rotation in our multiple scattering experiments [6].

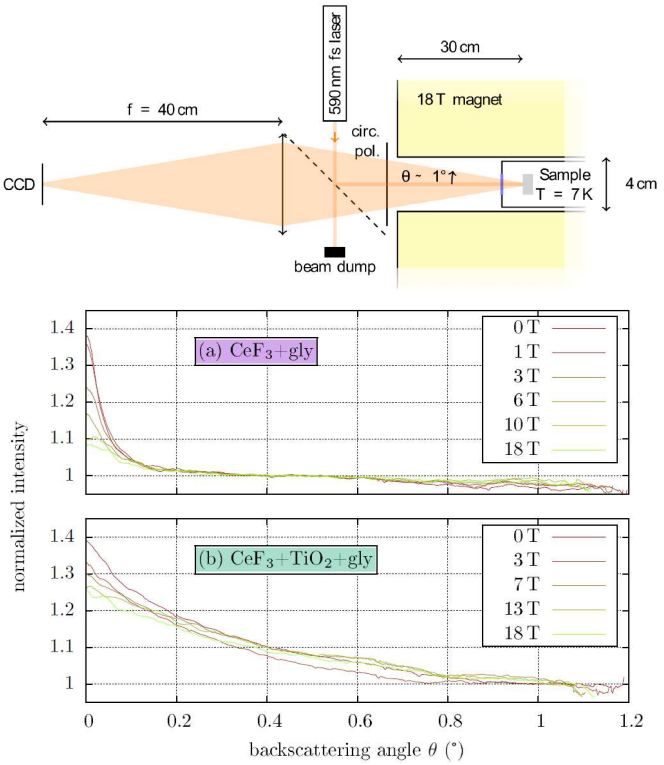

FIG. 16.1 – Top: Schematic CBC setup: A laser beam ($\lambda \approx 590$ nm) illuminates via a 50:50 beamsplitter a powder sample which is placed in a flow cryostat. The cryostat is located in a vertical bore 18 T magnet. A circular polarizer blocks single backscattered light. The reflected multiple scattered light is collected in k-space on a CCD via a lens (f = 40 cm) for scattering angles of up to $\theta \simeq 1°$. Bottom: CBC results for different magnetic fields between 0 and 18 T for a sample consisting of (a) 26 vol% CeF_3 powder mixed with glycerol and (b) 26 vol% CeF_3 powder mixed with 2 vol% TiO_2 powder and glycerol. Experiments were carried out at T = 7 K. Cones in (a) are normalized to a baseline between 0.4° and 0.5°. Cones in (b) are normalized to a baseline between 1.0° and 1.1°.

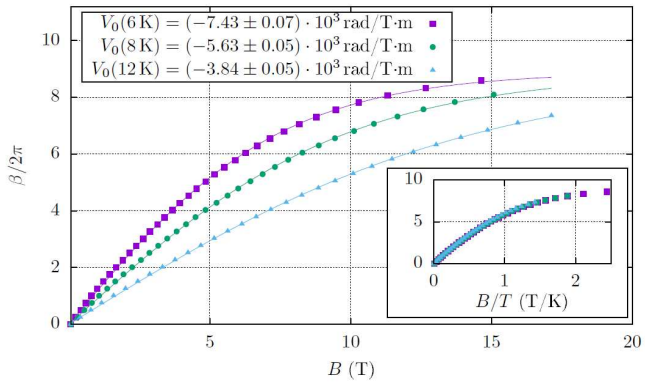

FIG. 16.2 – Faraday rotation angle β of a bulk crystal slab shaped sample (L = 1 mm) as a function of magnetic field at 6, 8 and 12 K. A 532 nm CW-laser was used for illumination. The data were fitted with $V_0 L \frac{T}{\alpha} \tanh(\frac{\alpha B}{T})$ to obtain the B = 0 bulk Verdet constant V_0 and the saturation parameter α (solid lines). For all three temperatures, $\alpha = (0.81 \pm 0.01)$ K/T. The inset shows that all the data collapse on a single curve when plotted as a function of B/T. The Verdet constant is proportional to the derivative of the curve and shows a saturation for high B/T ratios.

[1] P.W. Anderson, Phys. Rev. **109**, 5 (1958).

[2] Meint P. Van Albada and Ad Lagendijk, Phys. Rev. Lett. **55** 2692 (1985).

[3] Pierre-Etienne Wolf and Georg Maret, Phys. Rev. Lett. **55** 2696 (1985).

[4] S. Fiebig, C. M. Aegerter, W. Bührer, M. Störzer, E. Akkermans, G. Montambaux, and G. Maret, EPL (Europhysics Letters) **81** 64004 (2008).

[5] F. A. Erbacher, R. Lenke, and G. Maret, EPL (Europhysics Letters) **21** 551 (1993).

[6] L. Schertel, G. J. Aubry, C. M. Aegerter, and G. Maret, Europ. J. Phys. E to be published (2017).

16.2 Single-Plane Illumination Microscopy (SPIM) Using Spatial Light Modulation

In the past, we have used the principle of wave-front shaping in order to image structures behind turbid layers [7–9] as well as to control the illumination of a sample behind turbid layers [10]. The control of the light passed through turbid objects can also be used in modern forms of microscopy, where a light sheet is used to image single planes of a three dimensional sample with less photo-toxicity and higher speed than e.g. standard confocal microscopes [11, 12]. One problem with such single-plane illumination microscopes (SPIM) is that the quality of the light sheet often deteriorates quickly in deeper layers of a sample, such that only comparatively thin or transparent samples can be studied. We have now used dynamic wave-front shaping to create high quality light sheets even behind turbid layers that can be used to build a SPIM that works for situations with a turbid layer obscuring the sample of interest. The schematic setup using a technical phantom sample as a proof of principle is shown in Fig. 16.3. The illumination is from the front and is scrambled by a layer of tape attached to a glass slide. The sample consists of fluorescent beads in a glass capillary.

Using feedback from the detection objective 1, looking directly at the illumination light behind the sample, we form a light sheet in this illumination using a genetic algorithm changing the phase mask on a spatial light modulator (SLM) in the illumination path. We then obtain a narrow light sheet extending more than

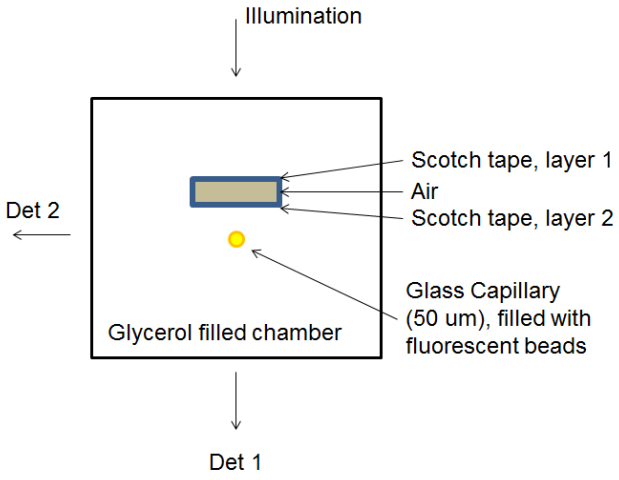

FIG. 16.3 – Schematic setup of a single-plane illumination microscopes (SPIM) behind turbid layers. The illuminating light is observed with detecting objective 1, where we can also observe the fluorescence of the particles imaged. The light sheet is observed using detection objective 2, at right angles to the illumination.

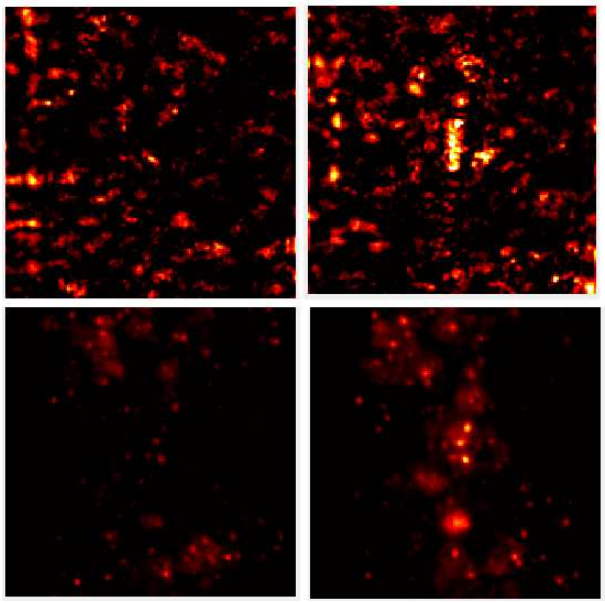

FIG. 16.4 – Creation of a dynamic light sheet behind a turbid layer. Top: transmission speckle pattern observed by detection objective 1, before (left) and after (right) application of a phase mask onto the spatial light modulator (SLM). The optimisation algorithm targets a line in the field of view for increased contrast, which corresponds to the light sheet used for illumination below (see Fig. 16.5). Bottom: fluorescence signal observed by detection objective 1 before (left) and after (right) application of the optimisation phase mask onto the SLM. The fluorescent particles within the light sheet are enhanced after application of the phase mask.

10 µm in the transverse direction. This is shown in the top panels of Fig. 16.4, where the direct illuminating light before and after application of the phase mask is shown. The corresponding fluorescent signal is shown in the bottom panels of Fig. 16.4, which clearly shows that fluorescent particles are more strongly illuminated by the light sheet.

This fluorescent signal can also be observed using detection objective 2 at right angles to the illumination, thus marking the entire depth of the sample in the field of view. This is shown in Fig.16.5, again before and after application of the phase mask to the spatial light modulator. As can be clearly seen, the creation of a light sheet in this situation leads to a drastically increased quality of the obtained image in a situation where a normal light sheet microscope would not be able to image, due to the multiple scattering of the turbid layer in front of the region of interest [13].

In conclusion, we have shown that wave-front shaping is capable of creating light-sheet imaging behind turbid layers at high resolution.

[7] I. M. Vellekoop and C. M. Aegerter, Opt. Lett. **35**, 1245 (2010).

[8] G. Ghielmetti and C. M. Aegerter, Opt. Express **20**, 3744 (2012).

[9] G. Ghielmetti and C .M. Aegerter, Opt. Express **22**, 1981 (2014). Science 305, 1007 (2004).

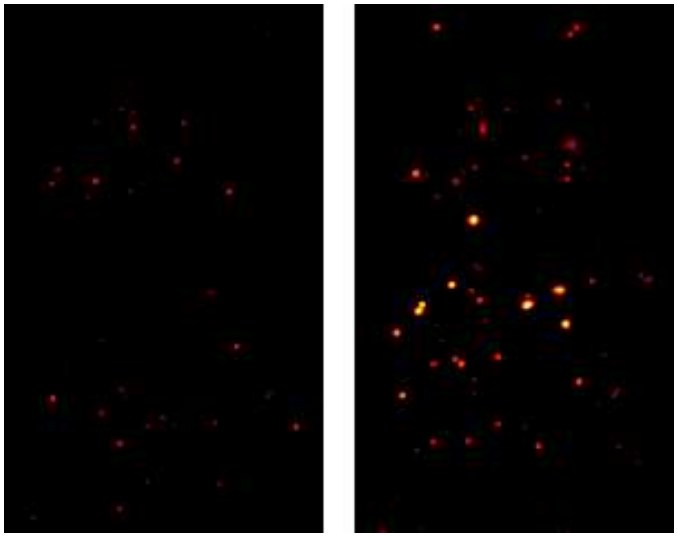

FIG. 16.5 – Fluorescent particles imaged with a light sheet behind a turbid layer using detection objective 2. The left panel shows the situation before application of the optimisation phase mask, whereas the right panel shows the situation after application of the phase mask. The fluorescent particles within the full depth of the light sheet are illuminated more strongly and allow for a depth resolved determination of the fluorescent structure.

[10] A. Malavalli, M. Ackermann, C. M. Aegerter, Opt. Express (2016).

[11] J. Huisken, J. Swoger, F. D. Bene, J. Wittbrodt, and E. H. K. Stelzer, Science 305, 1007 (2004).

[12] U. Krzic, S. Gunther, T.E. Saunders, S. J. Streichan, L. Hufnagel, Nat. Methods **9**, 730 (2012).

[13] J. Schneider and C. M. Aegerter to be published (2017).

16.3 FRET-Based Molecular Force Sensors in Drosophila Tissues

In the past, we have investigated the influence of mechanical forces on growth regulation and development in the wing imaginal disc of Drosophila, both theoretically [14,15] and experimentally [16,17]. In order to study the influence of tissue wide forces more directly on a cellular level, we have recently been active in the creation of molecular force sensors based on Forster resonance energy transfer (FRET) between two different fluorophores (in our case enhanced cyan and yellow fluorescent proteins, ECFP and EYFP, respectively) connected using an elastic linker and incorporated into a tension carrying structure of cell-cell contacts (E-Cadherin) [18]. The principle is illustrated in Fig. 16.6 A. As a control for the proper working of the construct as a force sensor, we have also introduced the same construct outside of the tension carrying structures of the cell-cell contacts, see Fig. 16.6 B.

When introducing the genetically altered construct of the adherens junction molecule into tissues of the Drosophila wing imaginal disc, we could observe resonance transfer by way of studying the change in intensity of the two different fluorophores, see Fig. 16.6 C, showing a difference between the sensor and control constructs. However, the efficiency in the control construct was lower than the sensor construct, which is contrary to the expectation that in the absence of a tension on the contact, the FRET efficiency should be higher due to the closer proximity of the fluorophores. The results in Fig. 16.6 C and D are an ensemble average over the whole tissue, whereas cell-cell junctions can show widely varying tensile forces acting on them, even in different parts of the cell. This is illustrated in Fig. 16.7 A for differently deformed cells. In order to account for such effects, we have studied the FRET efficiency for different segments of a cell boundary as well as for differently sized cells, see Fig. 16.7 A. As in the previous case, we have not found a significant difference between different types of cell junctions or between the sensor and control constructs.

To study this finding in more detail, in particular whether this is due to the absence of forces in the wing disc tissue, we have performed several determinations of the FRET efficiency in wing disc tissues with a direct change in the mechanical tension across the tissue. These were both biochemical and mechanical, increasing and decreasing the tension. The results of these experiments

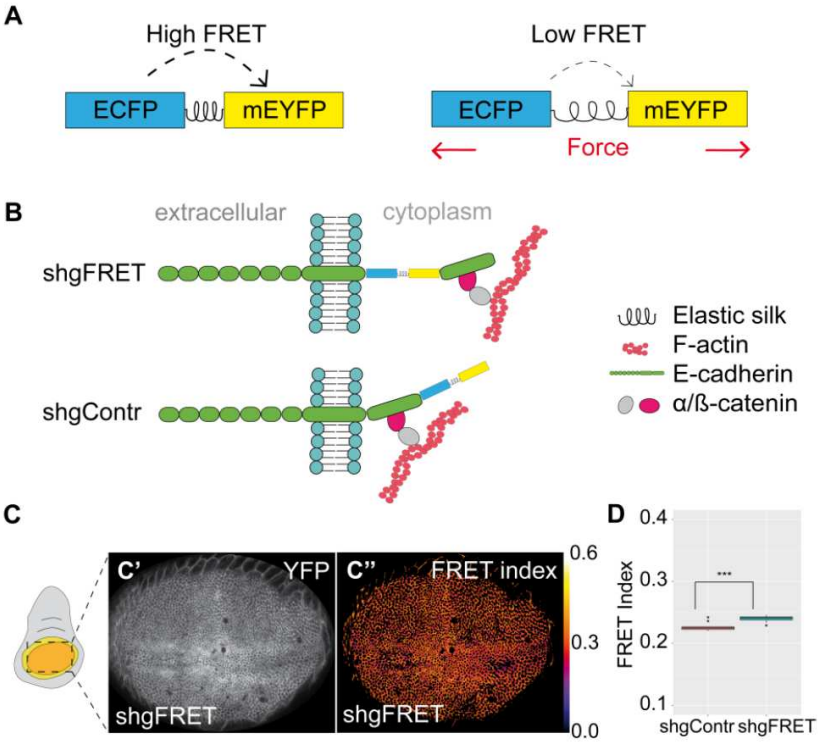

FIG. 16.6 – (A) The tension sensor consists of ECFP and mEYFP connected by an elastic linker (GPGGA)8. The FRET efficiency is high in a relaxed state but should decrease if external forces extend the sensor module.
(B) The sensor module was either integrated into the cytoplasmic domain of E-Cadherin adjacent to the transmembrane domain (shgFRET) to measure forces along the protein. The sensor module was also attached at the C-terminus of E-Cadherin (shgContr) lying outside of the force transducing domain to serve as a zero-force control.
(C) YFP expression (C') and corresponding FRET index (C'') of shgFRET shows that FRET was detectable in the wing pouch.
(D) FRET index in the wing pouch of shgContr (0.227, n=10) was significantly lower than for shgFRET (0.240, n=10).

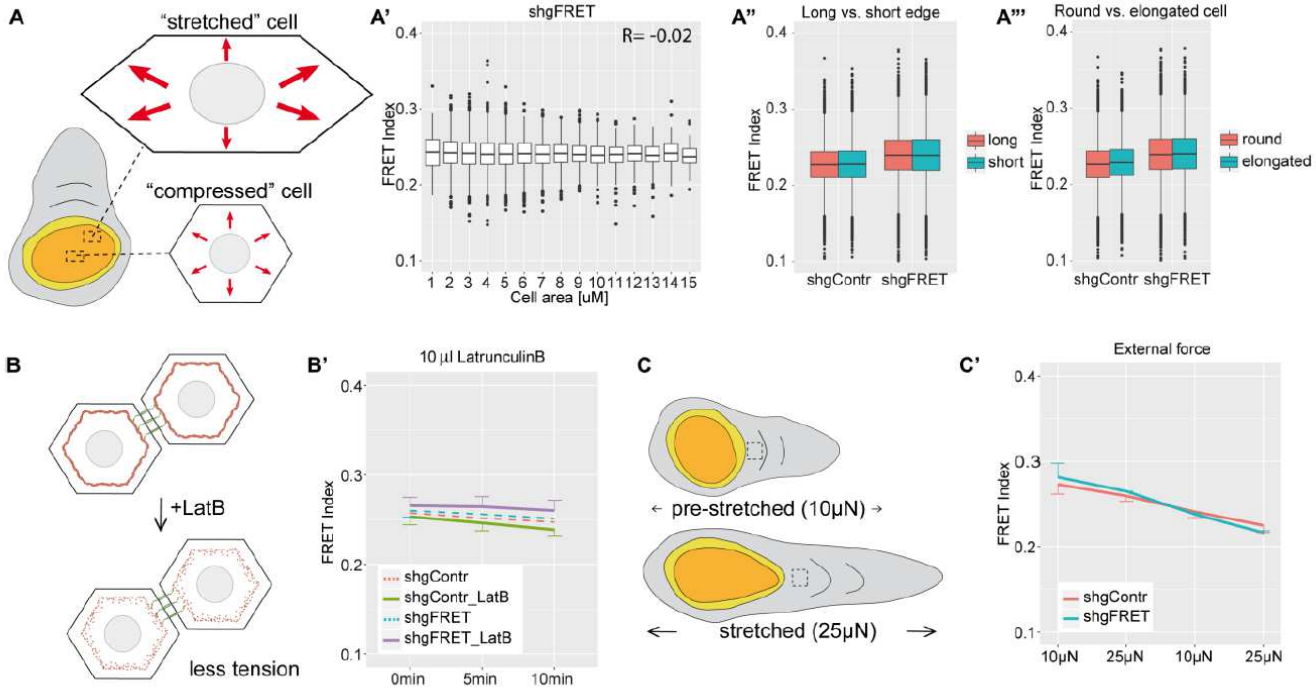

FIG. 16.7 – (A) Schematic drawing illustrates that cells in the center of the pouch are small, round and supposed to be mechanically compressed, whereas marginal cells are larger, elongated and mechanically stretched. In the marginal cells, the short edges are exposed to more mechanical stress than the long edges. These assumptions lead to following comparisons:
(A') The FRET index did not correlate with cell area in the wing pouch (here shown for shgFRET).
(A'') The FRET index did not differ between long and short edges for shgContr (0.228 vs. 0,227) and shgFRET (0.240 vs. 0.240).
(A''') The FRET index did not differ between round and elongated cells for shgContr (0.229 vs. 0.226) and shgFRET (0.240 vs. 0.240). (Data for $A', A''andA'''$ were pooled from 14 wing discs.)
(B) LatrunculinB treatment reduces cortical tension.
(B') FRET index decreased for shgContr (6%, n=18) and shgFRET(2%, n=18) upon treatment within 10 minutes. But also without treatment (dashed lines) the FRET index decreased over time for shgContr (4%, n=9) and shgFRET (3%, n=9).
(C) Using a stretching device, a pre-stretched (applied force of 10µN) and a stretched (25 µN) wind disc were compared. The dashed rectangle indicates the analyzed area.
(C') When cyclically altered between the two states of stretching every 5 minutes, a strong decay over time was observed for shgContr (18%, n=2) and shgFRET (23%, n=2), but no impact of the force change.

are visible in Fig. 16.7 B and C, indicating that both the sensor and the control construct show the same response to an applied force and that this response is also independent of the sign of the applied force. This indicates that either the sensor construct does not fulfill its function or the obtained FRET response is too small to be observed by the crude method of determining intensity ratios of the fluorophores, which is inherently sensitive to large systematic errors based in intensity fluctuations, photodetector efficiency etc.

In order to study the influence of systematic errors of the ratiometric FRET determination, we have also studied the efficiency of fluorescence transfer directly by measuring the fluorescent lifetime changes in the sensor and control constructs respectively. This has been done using a pulsed laser excitation and a time correlated photon counting module on a confocal microscope. In the presence of FRET, the lifetime of the donor fluorophore decreases, independent of any intensity-based imaging artifacts. The results are shown in Fig. 16.8 A, where the fluorescent lifetime of the donor (CFP) is shown for both constructs as well as in the absence of an acceptor fluorophore.

As can be seen by the decrease of the lifetime of the constructs relative to the pure donor fluorophore, FRET is taking place at small efficiency, however the comparison between the sensor and control constructs shows that this is irrespective of the mechanical tension carried by the construct. This implies that the construct does not

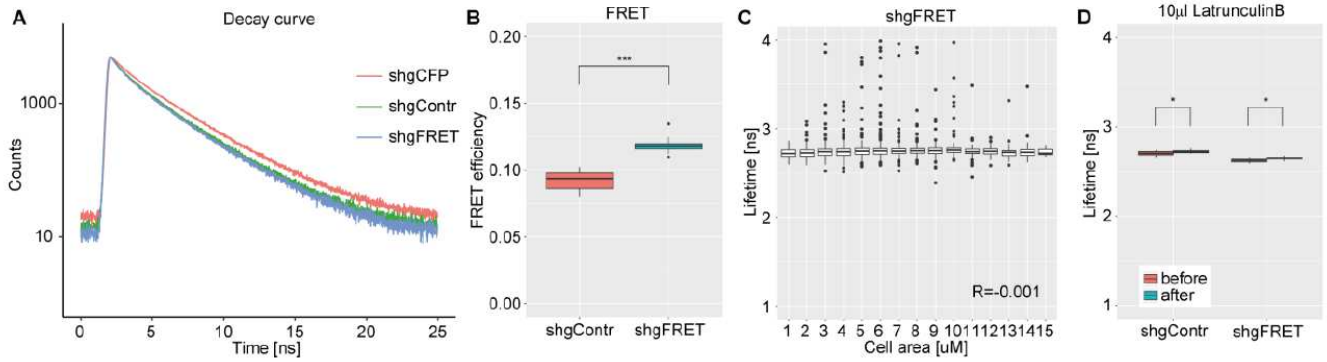

FIG. 16.8 – (A) Fluorescence decay curves of shgContr and shgFRET were almost overlapping, and both revealed lower lifetimes than shgCFP (n=5).
(B) Calculated FRET efficiency was significantly lower for shgContr (0.09, n=15) than for shgFRET (0.12, n=14).
(C) Lifetimes of single cells in the wing pouch did not correlate with cell size (here for shgFRET, n=8 wing discs).
(D) Lowering tensions by LatrunculinB treatment similarly increased lifetimes of shgContr and shgFRET for 1% (n=9).

work as a tension sensor, but rather the FRET signal is quenched either by angular conformations within the crowded cell environment or by intermolecular FRET of neighbouring molecules.

These findings are in contrast to earlier studies of a similar construct used in cell migration in the Drosophila oocyte, which has found differences in mechanical tension in different migrating situations [19]. To test for this, we have used the molecular force sensor in the same tissue of migrating cells, as well as in dorsal closure in the embryo, where large cellular forces are at work. In neither case could we find that the control construct gives different results from the sensor construct. We have also used the same construct as [19] and could not replicate their findings.

Thus, we conclude that in the crowded environment of a cell and a tissue, the FRET based molecular force sensor cannot be used as a measure of mechanical tension.

[14] T. Aegerter-Wilmsen, C.M. Aegerter, E. Hafen, and K. Basler,
Mechanisms of Development **124**, 318 (2007).

[15] T. Aegerter-Wilmsen, M.B. Heimlicher, A.C. Smith, P. Barbier de Reuille, R.S. Smith, C.M. Aegerter, and K. Basler,
Development **139** 3221 (2012).

[16] T. Schluck, U. Nienhaus, T. Aegerter-Wilmsen, and C.M. Aegerter,
PLoS One **8**, e76171 (2013).

[17] U. Nienhaus, T. Aegerter-Wilmsen, and C.M. Aegerter,
Mechanisms of Development **126**, 942 (2009).

[18] C. Grashoff, B.D. Hoffman, M.D. Brenner, R. Zhou, M. Parsons, M.T. Yang, M.A. McLean, S.G. Sligar, C.S. Chen, T. Ha, and M.A. Schwartz,
Nature **466**, 263 (2010).

[19] D. Cai, S.-C. Chen, M. Prasad, L. He, X. Wang, V. Choesmel-Cadamuro, J.K. Sawyer, G. Danuser, and D.J. Montell, Cell **157**, 1146 (2014).

[20] D. Eder, K. Basler, and C.M. Aegerter,
Sci. Reports to be published (2017).